Confocal Raman data analysis of tufts and spindles at the human dentin-enamel junction

Alban Desoutter, Amel Slimani, Hervé Tassery, Frédéric Cuisinier, Salavatore Sauro, Hamideh Salehi, Ivan Panayotov

Version of Record: https://www.sciencedirect.com/science/article/pii/S0003996921002259
Manuscript_11720c0d2792bca2caef7b9c7b981870

CONFOCAL RAMAN DATA ANALYSIS OF TUFTS AND SPINDLES AT THE HUMAN DENTIN-ENAMEL JUNCTION

Desoutter Alban[1], Amel Slimani[1], Tassery Hervé[1-2], Cuisinier Frédéric[1], Salavatore Sauro[3], Hamideh Salehi[1], Panayotov Ivan[1]

[1]*LBN, Univ Montpellier, Montpellier, France*

[2]*Université d'Aix-Marseille, Marseille, France.*

[3]*Facultad de Ciencias de la Salud Universidad CEU-Cardenal Herrera Valencia, Spain.*

Corresponding author: Alban Desoutter, LBN, UR UM104, 545 avenue du professeur Jean Louis Viala, 34193 Montpellier Cedex 5.

Abstract:

Objective: The aim of this article is to analyze the chemical mapping of tufts and spindles of the human dental enamel using confocal Raman microscopy measuring length, structuration and composition of spindles and tufts.

Design: we used Raman diffusion, based on the interaction between photons and optic phonons, to reveal chemical bound. Adult molars were selected and longitudinally sectioned. Areas of 120*120 micrometers were scanned near the dentin-enamel junction and grooves. Spectra were collected and phosphate and proteins peak intensities images were

reconstructed, related to HPA concentration. Images of Phosphate (PO_4^{3-}, 960cm^{-1}) and protein (CH, 2800/3000cm^{-1}) intensities have been reconstructed. K-mean cluster has been calculated to compare centroid spectra from enamel, dentin and tuft or spindle.

Results: intensity profile revealed spindles as less mineralized areas than enamel, from 5 to 10 micrometers large. In the groove of molar, long tufts were found, more than 150 micrometers.

Conclusions: Confocal Raman microscopy is a very interesting tool to characterize chemically secondary structure of enamel. The size of a tuft in the groove allows us make the hypothesis that they could play a role in long term resilience of mechanical stress.

Keywords: dentin enamel junction, confocal Raman microscopy, mineralized tissues, enamel, dentin, tuft, spindles

INTRODUCTION

Dentin-enamel junction (DEJ) is the transitional zone between two main human tooth components, dentin and enamel. It has specific characteristics that allow an interaction between two dissimilar calcified dental tissues in terms of composition and chemico-physical properties. Indeed, enamel is made of hydroxyapatite crystals (approx. 96 wt%), and of enamel-specific developmental proteins (1–2 wt%) such as enamelins bounded to hydroxyapatite crystals (Fincham et al., 1999; Robinson et al., 1998). Conversely, dentine is made of 50–70 vol% calcium-deficient and carbonate-rich hydroxyapatite [HAP: $Ca_{10}(PO_4)_6(OH)_2$]. The apatite crystal size in dentine (5x30x100 nm^3) is smaller than in enamel (G. W. Marshall, 1993), with less calcium than stoichiometric HAP, but also contains 4–5% of carbonates. Dentine contains also 30% of organic components which is represented by: i) 90% type I collagen with a very minimal amount of type III and V collagen, and 10% water-rich non-collagenous proteins (NCPs) such as proteoglycans and glycosaminoglycans; ii) 20% of the volume of the dentine is made of free (e.g., intratubular fluid) and bounded water.

The DEJ plays an important role in particular for the prevention of crack propagation from enamel into dentin, as for the propagation of the caries process.

The DEJ is characterized by an enamel organic matrix (EOM) that contains several proteins with multiple functions as the calcium ion-binding, the formation of extracellular matrix, cytoskeleton, cytoskeletal protein binding, cell adhesion, and transport. The main protein is collagen type, while some traces of ameloblastin and amelogenin were also found in recent work on proteomic in human enamel teeth (Jágr et al., 2019).

Previous studies identified differences in the molecular structural of both mineral and organic matrix across the DEJ using two dimensional confocal Raman micro spectroscopic mapping (Xu et al., 2009), micro hardness and toughness (Marshall Jr et al., 2001) auto-fluorescence scanning (Gallagher et al., 2003) FTIR imaging (Verdelis et al., 2003) and phosphate content using confocal Raman spectroscopy (Slimani et al., 2017). Indeed, the DEJ showed a three-level structure composed by :1) zone characterized by a 25–100 µm scallops (Brauer et al., 2010) with their convexities directed toward the dentin and concavities toward the enamel, 2) a zone with 2–5 µm micro-scallops and 3) a zone with even smaller structures. The functional dimension of the DEJ (between dentin and enamel) was demonstrated with AFM nano-indentation to be of 11.8 µm, while the smaller probe used for AFM nano-scratching yielded to a dimension of the DEJ of 2.0 µm. Conversely, the microRaman analysis yielded to a width of 7.0 µm (S. J. Marshall et al., 2003).

Moreover, a novel organic protein-containing enamel matrix layer (OM) was also identified using scanning electron microscopy and Raman spectroscopy of etched buccal-lingual sections of teeth crowns (Dusevich et al., 2012a). This layer looks like a three-dimensional fibrous meshwork with a different aspect compared to conventional enamel tufts. These latter are in fact smaller with branching defects that are found exclusively at the DEJ, protruding towards the enamel surface. They are well described by histological images or scanning electron microscope visualization (Amizuka et al., 2005). However, there is an evident confusion between enamel lamellae and enamel spindles which are, in contrast to the tufts, continuous with odontoblast processes that extend into the enamel junction. Lamellae are linear enamel defects that extend from the surface of the enamel towards the DEJ and vice versa. Enamel spindle branched rarely. They are usually found to cross prism boundaries and some of them are found partially or totally occluded by small needle-like crystals (Palamara et al., 1989a). Another secondary structure in the DEJ zone is the spindle, a small prolongation

of tubuli in the first micrometers of inner enamel. Spindles and tufts represent areas of hypomineralization and partial remineralization with increased void volume. The EOM appears as sheath-like structures within the enamel interphase matrix and extended from the DEJ about 100-400 µm into the enamel region called cuspid, corresponding to the pointed top of tooth. During Raman analysis, it was observed a C-H stretching peak at 2931 cm^{-1} characteristic of proteins. This was correlated directly to the presence and location of the matrix layer, as previously identified by scanning electron microscopy (Dusevich et al., 2012a). Nevertheless, there is no study describing a complete micro-Raman spectroscopy analysis of the mineral/organic signals including phosphate, carbonate, amide I/II/III band assignments, ratios and cluster type analysis of this enamel organic matrix layer neither the bristly enamel tufts/spindles matrix.

Thus, the objective of this study was to investigate the chemical composition of the overall DEJ and specifically the bristly tufts and spindles mesh in the human enamel with an original micro-Raman spectroscopy analysis.

Confocal Raman microscopy a non-invasive label free technique that measures the inelastic scattering of incident light energy to analyze the structure of mineralized tissues. The spatial resolution of Raman microscopy (300 nm) provides a high-resolution chemical map of phosphate, carbonate and organic structure (Gallagher et al., 2003).

The role of such structures was discussed in recent literature about fundamental dental histology and in paleontology. Indeed, if the DEJ is considered as a factor of adaption of the teeth to reduce strain and prevent cracks during mastication, the role of those structures in the DEJ was evocated in a 2008 publication, about resilience and teeth (Chai et al., 2009). Another study explains the link between adaptation of the mechanical properties of teeth and primate dietary and in general, in mammalian evolution (Constantino et al., 2012).

A deeper look into such structures gives a better understanding of their mechanical role related to their chemical mineral/organic patterns. A biochemical map of the groove region (separation of two cuspids) in DEJ could confirm the reason for increasing flexibility and cracks prevention related to a hypomineralized zone. This method could be expanded to other joining dissimilar dental materials.

2. MATERIALS AND METHODS

2.1. Specimen preparation

Five human third molars, extracted for orthodontic treatments, were collected with patients informed consent (process No. 2014-2198 - local ethical research committee). Teeth were sectioned along the longitudinal axis using an automatized 700 micrometers thickness diamond saw (Isomet 2000, Buehler, Lake Bluff, USA) The specimens were polished using silicon carbide abrasive discs (#320, #800 and #1200) mounted on a polishing disc ESC 200GT (ESCIL®). The final polishing was performed with a diamond paste 1PS4 6PS4 (ESCIL® - (6 µm, 1 µm and 0.25 µm)) using a polishing Vito TW table (ESCIL®, Lyon, France) mounted on a magnetic SMA 200 (ESCIL ® Escil, Lyon, France). Finally, the specimens were treated for 280 s in an ultrasonic bath containing distilled water.

2.2. Raman Data Acquisition

Raman spectra analysis was performed a Witec Confocal Raman Microscope System alpha 300R (Witec Inc., Ulm, Germany). Excitation in the confocal Raman microscopy is achieved through Nd: YAG laser (Newport, Evry, France) with a wavelength of 532nm. The incident laser beam was focused onto the surface of the specimens using a ×20 NIKON objective (Nikon, Tokyo, Japan). Then Raman backscattered radiation mixed with Rayleigh scattered

were passed through an edge filter to block the Rayleigh's. Acquisition time of a single spectrum was set to 0.5 s. 150 x 150 points per image and the analysis was executed using a piezoelectric table, leading to a total of 22,500 spectra for each image; each spectrum corresponded to a spatial unit (defined as: voxel). Data acquisition was performed using Image Plus software from Witec.

2.3 Data Analysis

Data analysis was performed using two methods. The first method provided integrated Raman intensities in specific regions at particular peaks. Data processing was performed using Image Plus software 5.2 from Witec. Each image regarding such integrated intensities provided a map of the region. Using a "look-up" table, each color showed different Raman peak intensity, which represented different intensity of phosphate, carbonate or organic components. For instance, dark hues were characteristic for low intensities of a specific element, while the yellow color indicated great presence of selected region.

The second method was based on a graph calculator and an Image Cross Section. It was realized using the Witec Project Plus 5.2 (Ulm, Germany) software. An image representing a ratio of two different reconstructed images/elements was reconsctucted using Witec Project Plus software. At each pixel, a number with a corresponding color showed the ratio of two peaks at a specific point/position of the specimen.

This second method was based on a K-mean cluster analysis (KMCA, Witec Project Plus software, Ulm, Germany)), which was able to find a partition where objects within each cluster were as close to each other as possible, and as far from objects in other clusters as possible.

3. RESULTS

A specific Raman spectrum of enamel and dentin is plotted to show the relative band assignments, (Fig 1A. and Table 1). As expected, some peaks are representative of organic parts. For example, the collagen presence is related to a high intensity of CH peak around 2800-3000 cm^{-1}. As shown, the phosphate rate is higher in enamel than in dentin.

[Figure 1]

[Table 1]

By filtering spectra with peaks intensities, Raman reconstructed images allow to visualize the organic and mineral distributions in the samples.

To present the distribution of different chemical composition in tufts and spindle, several Raman scans was realized. After data analysis, in Fig 2 for tufts, organic and phosphate map were plotted. An optical image shows the selected zone for scan. Each pixel in the image contains all information for further analysis to obtain different maps for phosphate vibrational mode and/ or carbonate and/or organic. Fig 2B/F represents a reconstructed image of the 960cm^{-1} Raman peak (phosphate PO_4^{3-}). Fig 2C/G reveal a reconstructed image relevant to Raman intensities of the 2800/3000 cm^{-1} peaks (protein groups C-H and CH_2). The grey/black area represents the dentin and the yellow/orange area is enamel. In between, the DEJ is represented by the broad region color coded in bleu/green. A lookup table is presented close to the chemical images to obtain the related intensities for each false color. Accordingly, Fig 3 the same data analysis was performed to present several spindle maps to improve the observation comparing to tuft distributions.

[Figure 2]

[Figure 3]

Fig. 4A represents two chemical images, with plotted lines on different zones of intersections started in dentin to inner structure, to quantify the variation of phosphate to organic along the lines. The images of collected intensities of the 960 cm^{-1} peak (phosphate PO_4^{3-}) and Raman intensities of 2800/3000 cm^{-1} organic peaks (protein groups: C-H, CH_2) calculated separately and the ratio of these two peaks are shown in the Fig 4A and 4C for different tufts. Several cross sections were plotted in Fig 4B and 4D to show clearly the difference of this variation along tuft and non-tuft zones.

[Figure 4]

Further analysis is done in Fig 5 to divide the different groups of spectra and present them in clusters: each color is presented with the same color average spectra. In Fig.5A two tufts are shown with reconstructed images for Raman intensities of the 960 cm^{-1} peak (ν_1 of PO_4^{3-}). For a better presentation four clusters gathering its spectra families are calculated in Fig 5B and in part C colored spectra of clusters shown. The same analysis is done for a spindle: in Fig 5D image of Raman intensities of the 960 cm^{-1} peak (ν_1 of PO_4^{3-}) of a spindle is given. In Fig 5E, cluster image with four spectra groups and average spectra are presented in Fig 5F.

[Figure 5]

4. DISCUSSION.

We obtained the spectra of different materials of tooth as expected. Indeed, characteristic peaks of enamel, dentin and DEJ are known (Tsuda et al., 1996) and our result confirm other previous work on human teeth scanned with a confocal Raman microscope (Desoutter et al., 2019).

The results of this study highlighted that enamel tufts are characterized by branches and projected within the DEJ, but with different composition at the dentin and enamel fronts (Fig 5). It is well known that enamel tufts are the results of a hypomineralization, as they are characterized by a low presence of phosphate in the structure. However, the phosphate content in enamel tufts is lower compared to sound enamel, but higher compared to dentin. The reconstructed images (Fig 2 and 3) based on the phosphate peak revealed a specific edge between the enamel and dentin, especially when considering the phosphate gradient. It was interesting to observe that the enamel tufts presented the same lever of mineralization of the inner zone of the DEJ. Moreover, the enamel tufts were surrounded by a crystalline structure especially in proximity of the enamel front. The Raman analysis of the organic vibration C-H, CH_2 revealed the data with shadow of the enamel tufts and spindles from the DEJ (Fig 2C/G and 3C/G). Unfortunately, the organic elements are undetectable in the enamel using Raman analysis; hence, these are shown in the analysis as dark grey/black areas. Conversely, the organic content increases along the dentin, it was then possible to observe. Raman stretching peas at 2931 cm^{-1}, which are characteristic of proteins (C-H, CH_2, CH_3, saturated acyl chains may also indicate the presence of triglyceride or phospholipids). The presence and the exact location of the matrix layer was also detected during scanning electron microscopy studies (Dusevich et al., 2012b), as well as the presence of collagen type VII (McGuire, Walker, et al., 2014) and IV (McGuire, Gorski, et al., 2014). An optical image the enamel tufts and spindles at the DEJ with marked scanned zones in the middle represents the interdigitation of the dentin and enamel tissues. The black square is the scanned area that acquired the Raman

spectra of the phosphate peak (PO_4^{3}, 960cm^{-1}) and produces the images for the relevant figures. The reconstructed Raman image of phosphate peak where the enamel tufts revealing their specific branched pattern with the highest intensity of phosphate in the enamel and the lowest content of phosphate in the dentin and in the center and the enamel tufts. The borders of the enamel tufts present an average intensity of phosphate, as if the mineralization of the enamel becomes more organized to intermingle with the surrounding normal enamel. The reconstructed Raman images obtained on the analysis of the protein's groups (C-H, CH_2 peaks: 2800/3000 cm^{-1}) – (Fig. 4A), showed almost no presence of organic components within the enamel, but these increase their presence at the DEJ and showed a maximum in dentin. The cluster (Fig 5B and E) of four spectra families validated the histological distinction between the dentin tubules and the enamel tufts, since the enamel tufts are related to a distinct cluster compared to the dentin tubuli~~n~~. This confirms the histological dissociation between the dentin tubules and the enamel tufts, which project from the DEJ into the enamel. The main advantages of Raman imaging are the need for no sample treatment such as etching, bleaching and fixing with glutaraldehyde.

In the optical images of the DEJ obtained in this study, the presence of cracks was often observed (Fig 3A) within the enamel; these were perpendicular to the DEJ line. However, these cracks appear to be enamel spindles. Raman images illustrate that tufts localized in the groove were clearly more evident and larger than those tufts or spindle localized in the cuspid zone. The size of tufts and spindle was not correctly studied in literature in such a cuspid zone, but it was advocated the these have a diameter of 2 µm (Palamara et al., 1989b). We observed that the tuft length from DEJ to the visible top area is 92 µm, but the structure seems continued out of image border. On the cuspid zone, the Raman reconstructed images showed spindle length of 7.32 µm (±2.19). The width was variable, from 6.2 micrometers on the first tuft, at the base, 4.3 micrometers for the second, and around 2.4 at the top. This diameter is

twice the diameter reported for tuft localized out of the groove. In accordance with previous studies (Boyde & Stewart, 1962; Boyde, 1984; Mills, 2014), the cross-section profile clearly showed that tuft are characterized by low mineralization; the phosphate intensity was 5.4 times higher in the sound enamel compared to the center of the tuft. Those outcomes may indicate the presence of tufts of large size, which may justify their low intensity of mineralization, compared to others DEJ areas. In conclusion, the presence of hypo mineralized tufts all around cuspid could store strain during jaw contraction. The huge resilience of teeth could be explained by the capacity of DEJ to increase the dumping of opposite forces on the enamel surface during mastication with, potential mechanical effects on the long term bonding strength of resin adhesive interface.

REFERENCES

Amizuka, N., Uchida, T., Nozawa-Inoue, K., Kawano, Y., Suzuki, A., Li, M., Nasu, M., Kojima, T., Sakagami, N., & Ozawa, H. (2005). Ultrastructural images of enamel tufts in human permanent teeth. *Journal of oral biosciences*, *47*(1), 33-41.

Boyde, A. (1984). Dependence of rate of physical erosion on orientation and density in mineralised tissues. *Anatomy and embryology*, *170*(1), 57-62.

Boyde, A., & Stewart, A. D. G. (1962). A study of the etching of dental tissues with argon ion beams. *Journal of ultrastructure research*, *7*(1-2), 159-172.

Brauer, D. S., Marshall, G. W., & Marshall, S. J. (2010). Variations in human DEJ scallop size with tooth type. *Journal of dentistry*, *38*(7), 597-601.

Chai, H., Lee, J. J.-W., Constantino, P. J., Lucas, P. W., & Lawn, B. R. (2009). Remarkable resilience of teeth. *Proceedings of the National Academy of Sciences*, *106*(18), 7289-7293.

Constantino, P. J., Lee, J. J.-W., Gerbig, Y., Hartstone-Rose, A., Talebi, M., Lawn, B. R., & Lucas, P. W. (2012). The role of tooth enamel mechanical properties in primate dietary adaptation. *American Journal of Physical Anthropology*, *148*(2), 171-177.

Desoutter, A., Slimani, A., Al-Obaidi, R., Barthélemi, S., Cuisinier, F., Tassery, H., & Salehi, H. (2019). Cross striation in human permanent and deciduous enamel measured with confocal Raman microscopy. *Journal of Raman Spectroscopy*, *50*(4), 548-556.

Dusevich, V., Xu, C., Wang, Y., Walker, M. P., & Gorski, J. P. (2012a). Identification of a protein-containing enamel matrix layer which bridges with the dentine–enamel junction of adult human teeth. *Archives of oral biology*, *57*(12), 1585-1594.

Dusevich, V., Xu, C., Wang, Y., Walker, M. P., & Gorski, J. P. (2012b). Identification of a protein-containing enamel matrix layer which bridges with the dentine–enamel junction of adult human teeth. *Archives of oral biology*, *57*(12), 1585-1594.

Fincham, A. G., Moradian-Oldak, J., & Simmer, J. P. (1999). The structural biology of the developing dental enamel matrix. *Journal of structural biology*, *126*(3), 270-299.

Gallagher, R. R., Demos, S. G., Balooch, M., Marshall Jr, G. W., & Marshall, S. J. (2003). Optical spectroscopy and imaging of the dentin–enamel junction in human third molars. *Journal of Biomedical Materials Research Part A: An Official Journal of The Society for Biomaterials, The Japanese Society for Biomaterials, and The Australian Society for Biomaterials and the Korean Society for Biomaterials*, *64*(2), 372-377.

Jágr, M., Ergang, P., Pataridis, S., Kolrosová, M., Bartoš, M., & Mikšík, I. (2019). Proteomic analysis of dentin–enamel junction and adjacent protein-containing enamel matrix layer of healthy human molar teeth. *European journal of oral sciences*, *127*(2), 112-121.

Marshall, G. W. (1993). Dentin : Microstructure and characterization. *Quintessence International (Berlin, Germany: 1985)*, *24*(9), 606-617.

Marshall Jr, G. W., Balooch, M., Gallagher, R. R., Gansky, S. A., & Marshall, S. J. (2001). Mechanical properties of the dentinoenamel junction : AFM studies of nanohardness, elastic modulus, and fracture. *Journal of Biomedical Materials Research: An Official Journal of The Society for Biomaterials and The Japanese Society for Biomaterials*, *54*(1), 87-95.

Marshall, S. J., Balooch, M., Habelitz, S., Balooch, G., Gallagher, R., & Marshall, G. W. (2003). The dentin–enamel junction—A natural, multilevel interface. *Journal of the European Ceramic Society*, *23*(15), 2897-2904.

McGuire, J. D., Gorski, J. P., Dusevich, V., Wang, Y., & Walker, M. P. (2014). Type IV Collagen is a Novel DEJ Biomarker that is Reduced by Radiotherapy. *Journal of Dental Research*, *93*(10), 1028-1034. https://doi.org/10.1177/0022034514548221

McGuire, J. D., Walker, M. P., Mousa, A., Wang, Y., & Gorski, J. P. (2014). Type VII collagen is enriched in the enamel organic matrix associated with the dentin–enamel junction of mature human teeth. *Bone*, *63*, 29-35. https://doi.org/10.1016/j.bone.2014.02.012

Mills, A. (2014). *Structural and chemical organization of teeth*. Elsevier.

Palamara, J., Phakey, P. P., Rachinger, W. A., & Orams, H. J. (1989a). The ultrastructure of spindles and tufts in human dental enamel. *Advances in dental research*, *3*(2), 249-257.

Palamara, J., Phakey, P. P., Rachinger, W. A., & Orams, H. J. (1989b). The ultrastructure of spindles and tufts in human dental enamel. *Advances in dental research*, *3*(2), 249-257.

Robinson, C., Brookes, S. J., Shore, R. C., & Kirkham, J. (1998). The developing enamel matrix : Nature and function. *European journal of oral sciences*, *106*(S1), 282-291.

Slimani, A., Nouioua, F., Desoutter, A., Levallois, B., Cuisinier, F. J., Tassery, H., Terrer, E., & Salehi, H. (2017). Confocal Raman mapping of collagen cross-link and crystallinity of human dentin–enamel junction. *Journal of Biomedical Optics*, *22*(8), 086003.

Tsuda, H., Ruben, J., & Arends, J. (1996). Raman spectra of human dentin mineral. *European journal of oral sciences*, *104*(2), 123-131.

Verdelis, K., Crenshaw, M. A., Paschalis, E. P., Doty, S., Atti, E., & Boskey, A. L. (2003). Spectroscopic imaging of mineral maturation in bovine dentin. *Journal of dental research*, *82*(9), 697-702.

Xu, C., Yao, X., Walker, M. P., & Wang, Y. (2009). Chemical/molecular structure of the dentin–enamel junction is dependent on the intratooth location. *Calcified tissue international*, *84*(3), 221.

Figure 1 Raman single spectrum of enamel and dentin. Each peak is connected to a chemical bond. 0 is connected to Rayleigh elastic diffusion, and other peaks are related to inelastic scattering, with a wavelength far from excitation laser wavelength.

Figure 2. Enamel tufts A) optical image 20× objective, the scanned zone is marked with black square; B) image of Raman intensities of the 960 cm^{-1} peak (ν_1 of PO_4^{3-}); C) Reconstructed image relevant to Raman intensities of the 2800/3000 cm^{-1} peaks (protein groups C-H and CH2) D) Intensity profiles related with black and red line in B) and C); right ordinate axis is connected with Phosphate intensity (black line) and left ordinate axis is connected with organic intensity (red line); E) optical image 20x, black square is scanned zone; F) Raman intensities of the 960 cm^{-1} peak (ν_1 of PO_4^{3-}); G) Reconstructed image relevant to Raman intensities of the 2800/3000 cm^{-1} peaks (protein groups C-H and CH2) H) Intensity profiles related with black and red line in E) and C); right ordinate axis is connected with Phosphate intensity (black line) and left ordinate axis is connected with organic intensity (red line); E) optical image 20x, black square is scanned zone.

Figure 3. Enamel spindles A) optical image 20× objective, black square is the scanned zone. B) Raman intensities of the 960 cm^{-1} peak (ν_1 of PO_4^{3-}); C) Reconstructed image relevant to Raman intensities of the 2800/3000 cm^{-1} peaks (protein groups C-H and CH2) D) Intensity profiles related with black and red line in B) and C); right ordinate axis is connected with Phosphate intensity (black line) and left ordinate axis is connected with organic intensity (red line); E) optical image 20x, black square is scanned zone; F) Raman intensities of the 960 cm^{-1} peak (ν_1 of PO_4^{3-}); G) Reconstructed image relevant to Raman intensities of the 2800/3000 cm^{-1} peaks (protein groups C-H and CH2) H) Intensity profiles related with black and red line in E) and C); right ordinate axis is connected with Phosphate intensity (black line) and left ordinate axis is connected with organic intensity (red line); E) optical image 20x, black square is scanned zone.

Figure 4. Enamel Tufts (A) Raman image of collected intensities of the 960 cm^{-1} peak (phosphate PO_4^{3-}) over Raman intensities of 2800/3000 cm^{-1} organic peaks (protein groups: C-H, CH_2) with two cross sections, red line and black line (B). Plotted variation of the phosphate to organic ratio along the two cross sections. (C) Raman image of collected intensities of the 960 cm^{-1} peak (phosphate PO_4^{3-}) over Raman intensities of 2800/3000 cm^{-1} organic peaks (protein groups: C-H, CH_2) with three cross sections, red line, black line and blue line. (D) Plotted variation of the phosphate to organic ratio along the three cross sections.

Figure 5 A) image of Raman intensities of the 960 cm^{-1} peak (ν_1 of PO_4^{3-}) of two tufts; B) Cluster picture gathering 4 spectra families; C) colored spectra of clusters shown in B); D) image of Raman intensities of the 960 cm^{-1} peak (ν_1 of PO_4^{3-}) of a spindle; E) Cluster picture gathering 4 spectra families, connected to D); F) colored spectra of clusters shown in E).

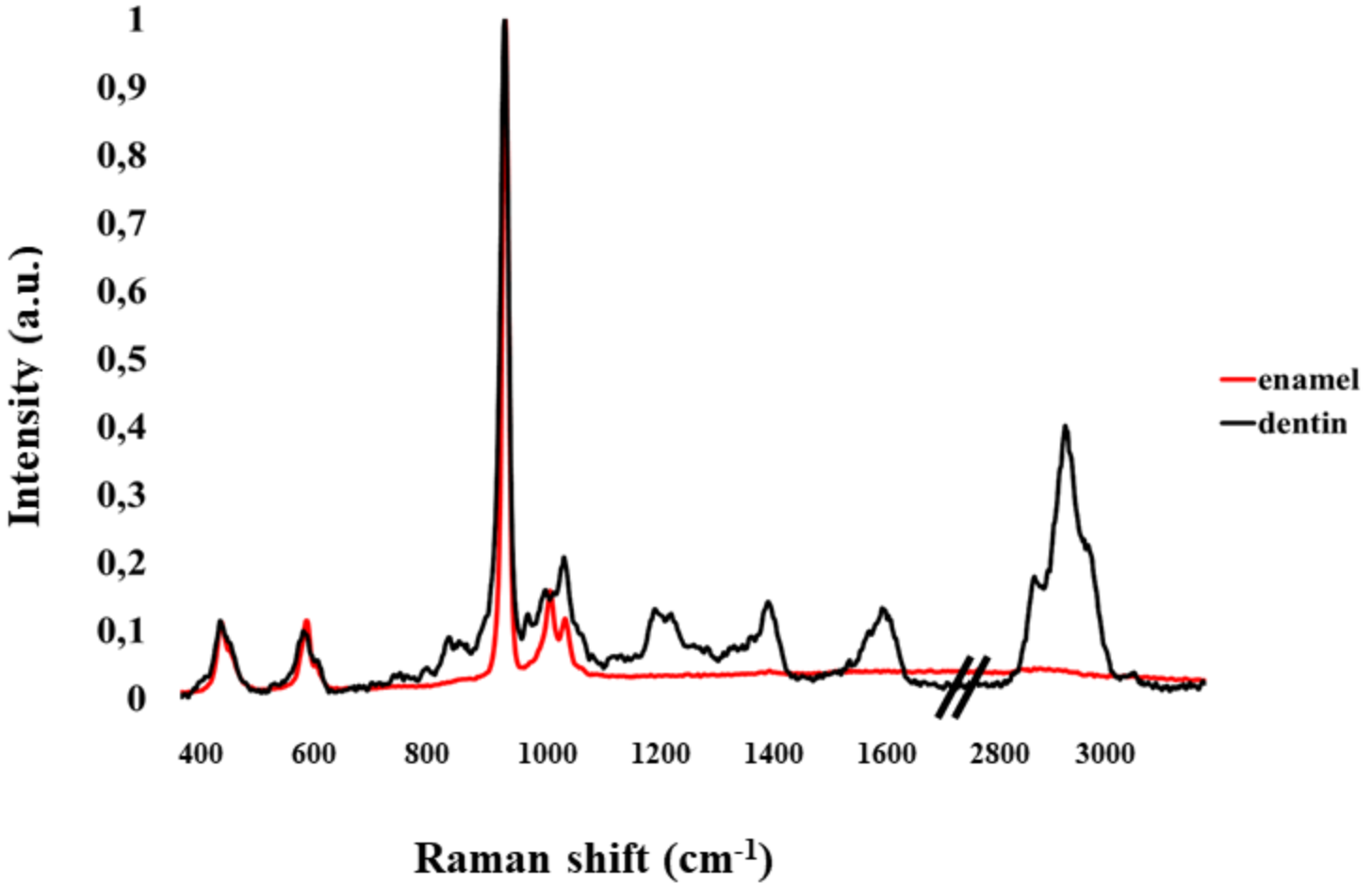
Intensity (a.u.)
1
0,9
0,8
0,7
0,6
0,5
0,4
0,3
0,2
0,1
0
400
600
800
1000
1200
1400
1600
2800
3000
Raman shift (cm-1)
enamel
dentin

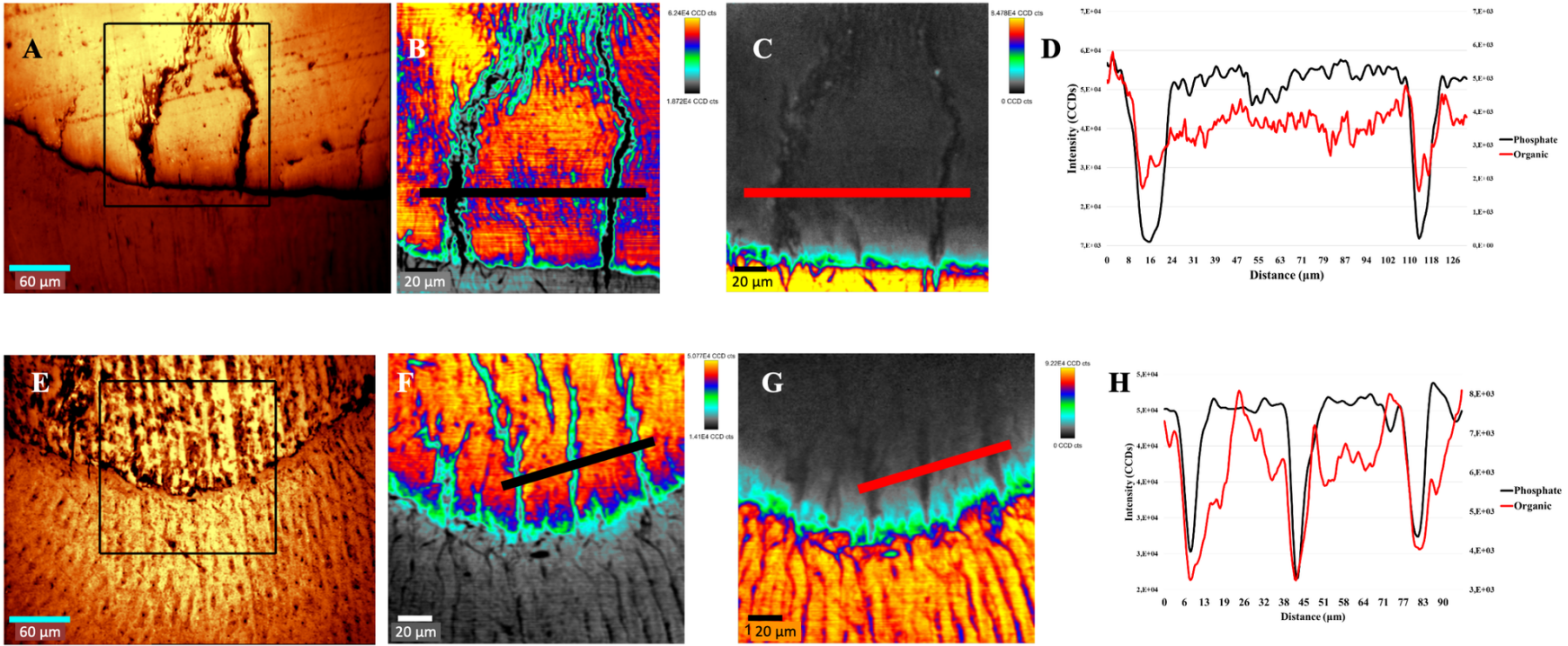
A
60 µm
B
6.24E4 CCD cts
1.872E4 CCD cts
20 µm
C
8.478E4 CCD cts
0 CCD cts
20 µm
D
Intensity (CCDs)
Distance (µm)
Phosphate
Organic
E
60 µm
F
5.077E4 CCD cts
1.41E4 CCD cts
20 µm
G
9.22E4 CCD cts
0 CCD cts
20 µm
H
Intensity (CCDs)
Distance (µm)
Phosphate
Organic

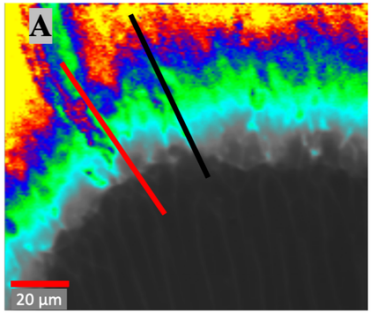
A
20 µm

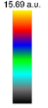
15.69 a.u.
0 a.u.

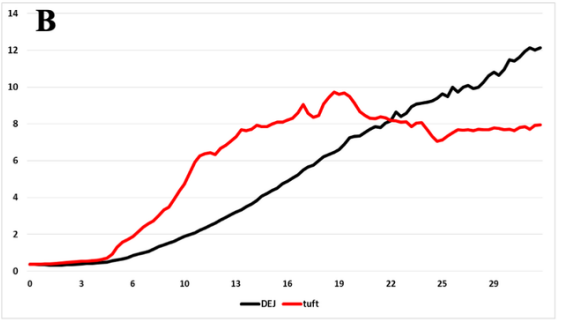
B
14
12
10
8
6
4
2
0
0
3
6
10
13
16
19
22
25
29
DEJ
tuft

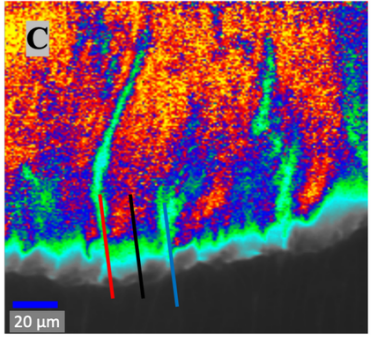
C
20 µm

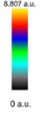
8.807 a.u.
0 a.u.

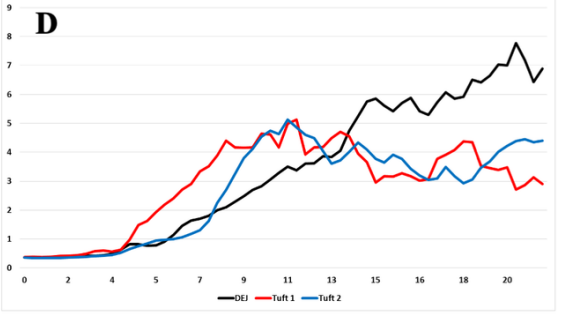
D
9
8
7
6
5
4
3
2
1
0
0
2
4
5
7
9
11
13
15
16
18
20
DEJ
Tuft 1
Tuft 2

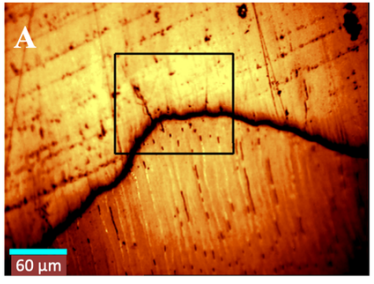
A
60 µm

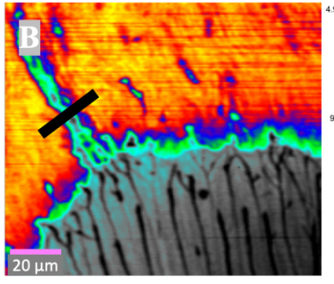
B
4.93E4 CCD cts
9246 CCD cts
20 µm

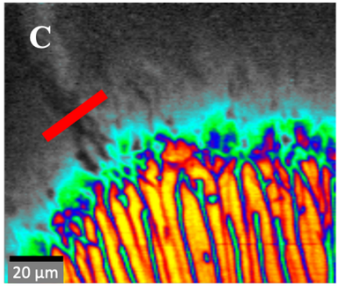
C
5.586E4 CCD cts
114 CCD cts
20 µm

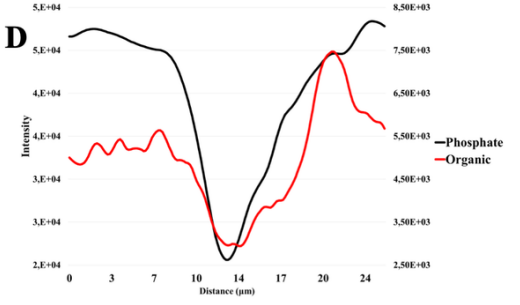
D
5,E+04
5,E+04
4,E+04
4,E+04
3,E+04
3,E+04
2,E+04
8,50E+03
7,50E+03
6,50E+03
5,50E+03
4,50E+03
3,50E+03
2,50E+03
Intensity
0
3
7
10
14
17
20
24
Distance (µm)
Phosphate
Organic

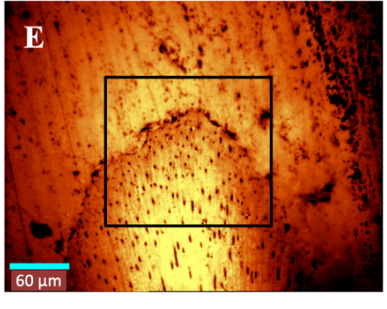
E
60 µm

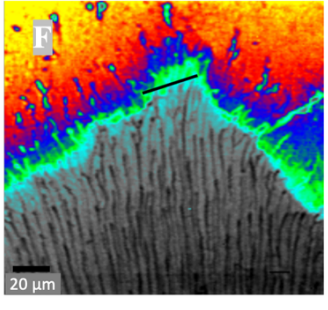
F
2.42E4 CCD cts
4129 CCD cts
20 µm

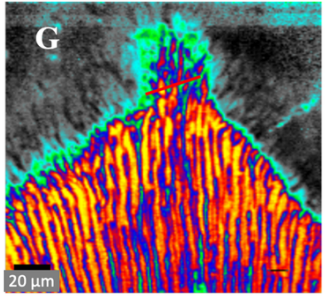
G
3.549E4 CCD cts
3340 CCD cts
20 µm

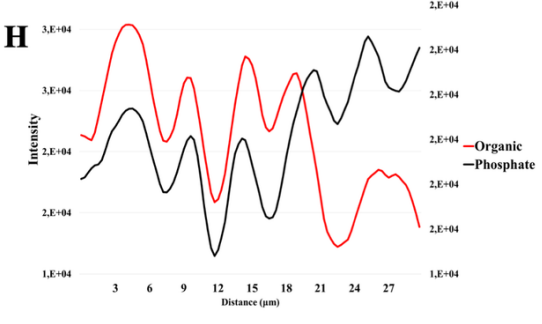
H
3,E+04
3,E+04
2,E+04
2,E+04
2,E+04
1,E+04
2,E+04
2,E+04
2,E+04
2,E+04
2,E+04
1,E+04
Intensity
3
6
9
12
15
18
21
24
27
Distance (µm)
Organic
Phosphate

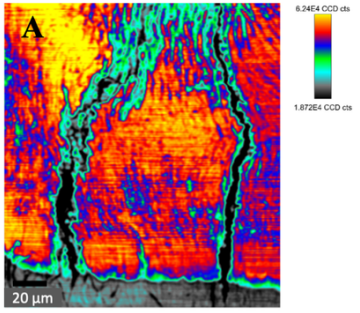
A
6.24E4 CCD cts
1.872E4 CCD cts
20 µm

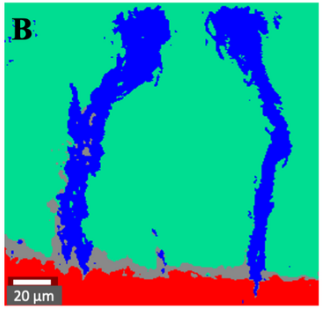
B
20 µm

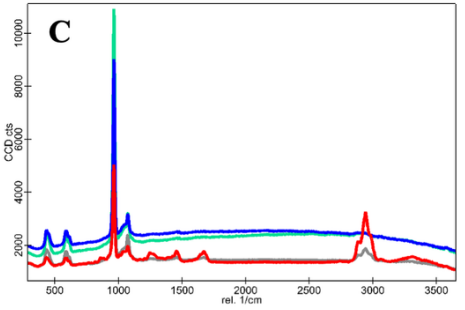
C
CCD cts
2000
4000
6000
8000
10000
500
1000
1500
2000
2500
3000
3500
rel. 1/cm

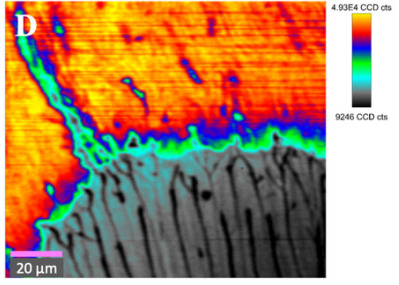
D
4.93E4 CCD cts
9246 CCD cts
20 µm

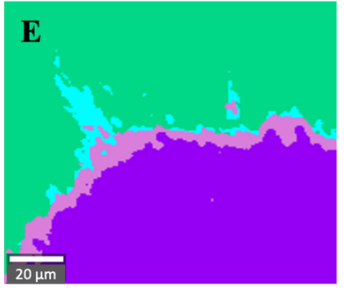
E
20 µm

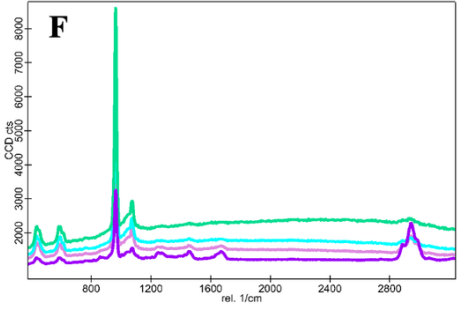
F
CCD cts
2000
3000
4000
5000
6000
7000
8000
800
1200
1600
2000
2400
2800
rel. 1/cm

Table 1. Table of enamel and dentin human tooth Raman peaks.

Band assignments of Raman spectra	Enamel	Dentin
	(Raman shift in cm-1)	
ν_2 Phosphate (PO_4^{3-})	433	432
ν_4 Phosphate (PO_4^{3-})	579-608	580-610
ν_1 Phosphate (PO_4^{3-})	960	960
B type ν_1 Phosphate (PO_4^{3-})	1071	1069
A type ν_2 Phosphate (PO_4^{3-})	1103	1102
(NH) Amide III		1243
(NH) Amide III non-polar triple helix of collagen		1275
CH (deformation)		1450
Amide I (C=O)		1665
Pentosidine		1550
AGEs		1550-1690
Phosphate to organic matrix ratios	960/1450	960/145
CH		2800-3000

AGEs: Advanced glycation end products ; ν_i: vibration mode of molecule.